

# A NAD-dependent glutamate dehydrogenase coordinates metabolism with cell division in *Caulobacter crescentus*

François Beaufay<sup>1</sup>, Jérôme Coppine<sup>1</sup>, Aurélie Mayard<sup>1</sup>, Géraldine Laloux<sup>2</sup>, Xavier De Bolle<sup>1</sup> & Régis Hallez<sup>1,\*</sup>

## Abstract

Coupling cell cycle with nutrient availability is a crucial process for all living cells. But how bacteria control cell division according to metabolic supplies remains poorly understood. Here, we describe a molecular mechanism that coordinates central metabolism with cell division in the  $\alpha$ -proteobacterium *Caulobacter crescentus*. This mechanism involves the NAD-dependent glutamate dehydrogenase GdhZ and the oxidoreductase-like KidO. While enzymatically active GdhZ directly interferes with FtsZ polymerization by stimulating its GTPase activity, KidO bound to NADH destabilizes lateral interactions between FtsZ protofilaments. Both GdhZ and KidO share the same regulatory network to concomitantly stimulate the rapid disassembly of the Z-ring, necessary for the subsequent release of progeny cells. Thus, this mechanism illustrates how proteins initially dedicated to metabolism coordinate cell cycle progression with nutrient availability.

**Keywords** cell division; cytokinesis; FtsZ; GdhZ; glutamate dehydrogenase

**Subject Categories** Metabolism; Cell Cycle; Microbiology, Virology & Host Pathogen Interaction

DOI 10.15252/emboj.201490730 | Received 5 December 2014 | Revised 14 April 2015 | Accepted 21 April 2015 | Published online 7 May 2015

The EMBO Journal (2015) 34: 1786–1800

## Introduction

Cell division is a key process to ensure survival, development, and spreading of all living beings. At the heart of this mechanism, self-assembly proteins play a crucial role (Margolin, 2000; Osteryoung, 2001). In eukaryotes, actin and myosin drive cell constriction, whereas microtubules form the mitotic spindle. In prokaryotes, the actin-like ATPase MreB and the tubulin-like GTPase FtsZ control cell growth and cytokinesis (Karsenti & Vernos, 2001; Margolin, 2009; Laporte *et al.*, 2010). Accordingly, self-assembly proteins are targeted by checkpoints all along the cell cycle. For instance,

cyclin-dependent kinases trigger the assembly of the mitotic spindle upon completion of DNA replication (Li & Zheng, 2004; Yokoyama & Gruss, 2013), while the nucleoid occlusion system inhibits FtsZ polymerization over the replicating chromosome and thereby prevents genome bisection (Wu & Errington, 2004; Bernhardt & de Boer, 2005). *In vitro*, FtsZ self-assembles in a GTP-dependent manner into protofilaments, which in turn associate through lateral interactions into structures of higher complexity (Mukherjee & Lutkenhaus, 1994; Erickson & Stoffler, 1996; Gonzalez *et al.*, 2003). *In vivo*, FtsZ assembles at the division site into a dynamic ring-like structure, called the Z-ring, where it acts as a scaffold for the recruitment of cell division proteins and plays an active role in cytokinesis (Goehring & Beckwith, 2005; Li *et al.*, 2007; Goley *et al.*, 2011). Although the exact molecular mechanism by which the Z-ring disassembly drives cell constriction *in vivo* is still under intense debate, GTPase activity and lateral interactions play a crucial role in this process (Monahan *et al.*, 2009; Dajkovic *et al.*, 2010; Erickson *et al.*, 2010; Osawa & Erickson, 2011). A recent study showed that the Z-ring is very likely continuous, composed of either overlapping shorter filaments or a single filament rolled up on itself (Szwedziak *et al.*, 2014). Most importantly, the authors proposed that cell constriction requires the filaments to slide along each other (Szwedziak *et al.*, 2014). Although lateral interactions between FtsZ filaments would play a direct role in this process, the GTPase activity might be crucial *in vivo* to initiate Z-ring disassembly as well as to maintain the dynamic state of the Z-ring, essentially by stimulating filament shrinkage (Stricker *et al.*, 2002; Osawa & Erickson, 2011; Szwedziak *et al.*, 2014).

The  $\alpha$ -proteobacterium *Caulobacter crescentus* is a powerful model to study cell division control since it divides asymmetrically to give rise to two different daughter cells, a small swarmer cell and a large stalked cell. The sessile stalked cell initiates DNA replication (S phase) shortly after the previous cytokinesis, whereas the motile swarmer cell first enters in a non-replicative G1 phase (Fig 1A). The swarmer cell then differentiates into a stalked cell by ejecting the polar flagellum, retracting the polar pili, and synthesizing a stalk at the same pole. This swarmer-to-stalked cell transition coincides with the initiation of DNA replication (G1-to-S transition). Although

<sup>1</sup> Bacterial Cell Cycle & Development (BCcD), URBM, University of Namur, Namur, Belgium

<sup>2</sup> de Duve Institute, Université catholique de Louvain, Brussels, Belgium

\*Corresponding author. Tel: +32 81 724 244; E-mail: regis.hallez@unamur.be

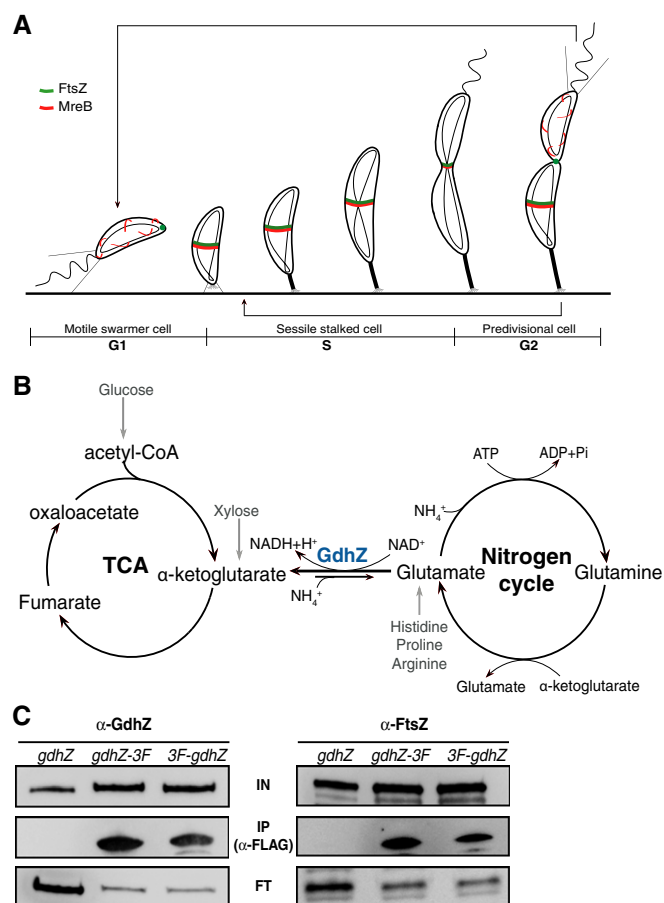


**Figure 1. The NAD-dependent glutamate dehydrogenase GdhZ interacts with FtsZ in *Caulobacter crescentus*.**

- A** *Caulobacter crescentus* cell cycle. During the G1 phase, the growth of the swarmer cell is controlled by the actin-like protein MreB (Aaron *et al.*, 2007) and FtsZ is localized at the new pole. Upon initiation of DNA replication (G1-to-S transition) and differentiation (swarmer-to-stalked transition), FtsZ polymerizes at midcell where it recruits MreB and all the other cell division proteins. Once DNA replication is complete, constriction starts at the end of the S phase to finally lead to septation (G2 phase) and the release of a small swarmer cell and a large stalked cell.
- B** GdhZ is a NAD-dependent glutamate dehydrogenase (GDH), which catalyzes the interconversion of glutamate into  $\alpha$ -ketoglutarate and ammonia, bridging the tricarboxylic acid cycle (TCA) with the nitrogen cycle. GdhZ is essential *in vivo* for the catabolism of histidine, proline, arginine, glutamine, and glutamate, since it constitutes the only entry point into the TCA.
- C** Co-immunoprecipitation (Co-IP) experiments showing that GdhZ can pull down FtsZ. Co-IP were performed on protein extracts of wild-type (RH50), *gdhZ-3FLAG* (RH728), and *3FLAG-gdhZ* (RH743) strains. GdhZ and FtsZ were detected by Western blotting using respectively anti-GdhZ and anti-FtsZ antibodies before (IN) and after immunoprecipitation (IP) with anti-FLAG antibodies. Proteins not immunoprecipitated were detected in flow-through (FT) fractions.

Source data are available online for this figure.

show that GdhZ (for glutamate dehydrogenase interacting with FtsZ) stimulates cell constriction during cytokinesis by directly interfering with Z-ring stability and that GDH activity is essential to mediate this effect. In addition, we found that GdhZ and KidO use different molecular mechanisms to stimulate depolymerization of FtsZ, but share the same regulatory network to synergistically prevent premature Z-ring formation in G1 swarmer cells and to trigger Z-ring disassembly in G2 predivisional cells. This mechanism illustrates how bacteria can adapt their cell cycle according to nutrient availability.

## Results

### A NAD-dependent glutamate dehydrogenase interacts with FtsZ

To find additional regulators of FtsZ, a yeast two-hybrid screen was performed using a prey library of random genomic DNA fragments of *C. crescentus* (see details in Supplementary Materials and Methods). We fished out a fragment encompassing the uncharacterized *CCNA\_00086* gene (here referred to as *gdhZ*), coding for a NAD-dependent GDH. To provide biochemical evidence that GdhZ and FtsZ are part of the same complex, lysates from strains in which *gdhZ* was replaced by either *3FLAG-gdhZ* or *gdhZ-3FLAG* were subjected to immunoprecipitation with  $\alpha$ -FLAG antibodies. These experiments showed that FtsZ was co-purified with both GdhZ fusions, further supporting the interaction between GdhZ and FtsZ (Fig 1C).

### *gdhZ* deletion leads to a severe cell division defect

By interacting with FtsZ, GdhZ might regulate cell division. To address this question, we first generated an in-frame deletion of *gdhZ* ( $\Delta$ *gdhZ*) and found that  $\Delta$ *gdhZ* cells displayed a large cell size heterogeneity with a high proportion of tiny and filamentous cells (Fig 2A and B). The  $\Delta$ *gdhZ* mutant also exhibited a serious growth defect, with a doubling time of ~165 min in complex media (PYE) compared

the Z-ring is built up at the onset of the S phase, cell constriction only starts at the early predivisional stage (late S phase) and is followed by a rapid contraction of the Z-ring in late predivisional stage (G2 phase) (Degnen & Newton, 1972; Osley & Newton, 1980; Holden *et al.*, 2014).

Among the regulators of FtsZ identified so far, only few have been described to coordinate cell division with metabolism (Kirkpatrick & Viollier, 2011). The glucosyltransferases, UgtP in *Bacillus subtilis* and OpgH in *Escherichia coli*, interfere with FtsZ dynamics to delay cell division, allowing cells to adapt their size according to nutrient availability (Weart *et al.*, 2007; Hill *et al.*, 2013). In contrast to *E. coli* or *B. subtilis*, *C. crescentus* does not vary its cell length in response to changes in nutrient availability (Campos *et al.*, 2014). Nevertheless, the small NAD(H)-binding protein KidO has been proposed to coordinate cell division with the metabolic state of the cell (Radhakrishnan *et al.*, 2010). KidO prevents premature Z-ring formation during G1 phase and promotes Z-ring disassembly in G2 phase, but cannot interfere with FtsZ during S phase since it is degraded by the ClpXP protease at the G1-to-S transition (Radhakrishnan *et al.*, 2010). However, the exact mechanism used by KidO to modulate FtsZ dynamics remains unknown.

Here, we identified a conserved bifunctional NAD-dependent glutamate dehydrogenase (GDH) that controls Z-ring disassembly. A GDH catalyzes the interconversion of glutamate into  $\alpha$ -ketoglutarate and ammonia by using NAD(P)H as a cofactor, thereby bridging Krebs and nitrogen cycles (Fig 1B) (Minambres *et al.*, 2000). We

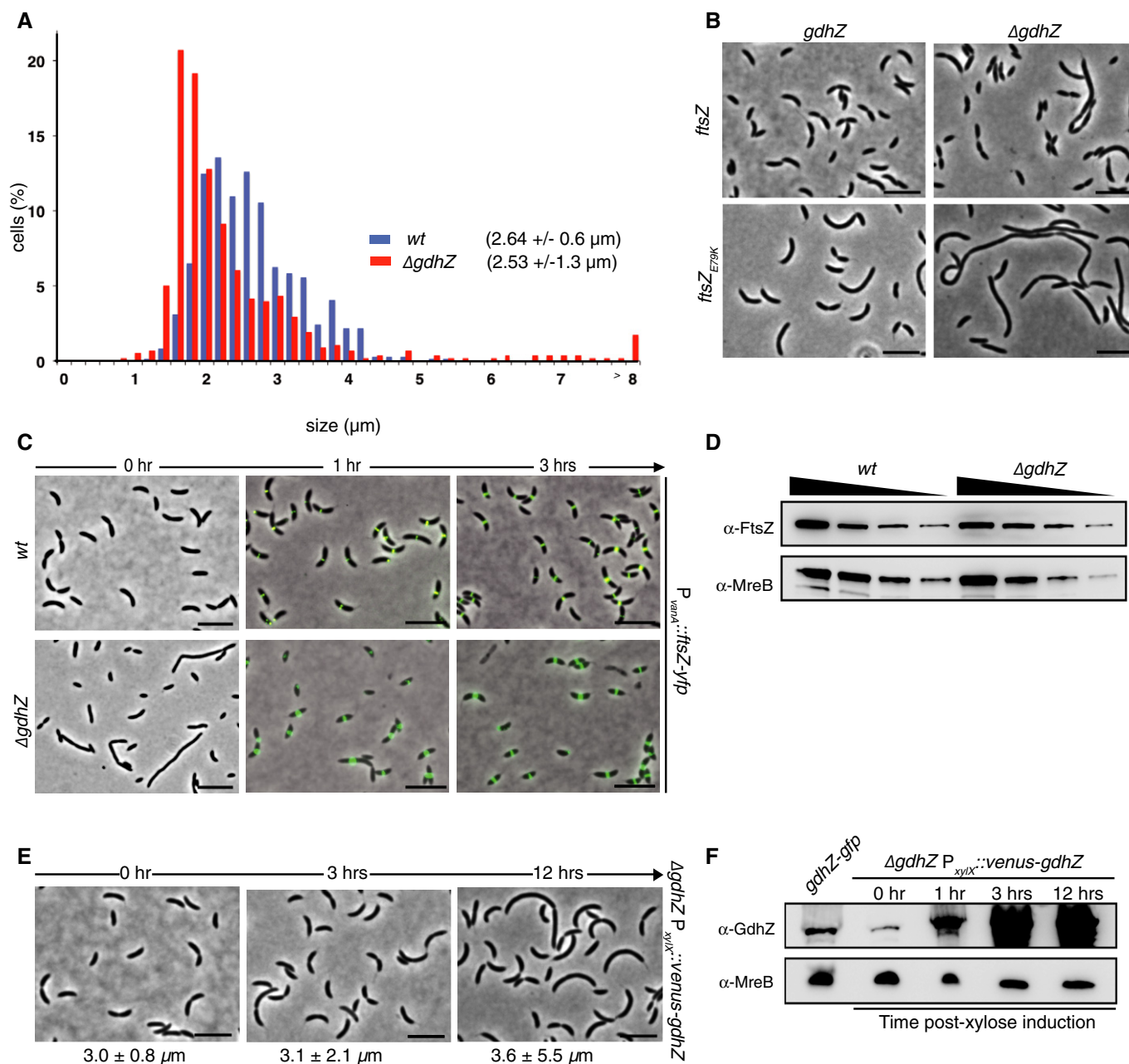


**Figure 2. Inactivation of *gdhZ* leads to a severe cell division defect.**

**A** Cell size distribution of wild-type (RH50) and  $\Delta\text{gdhZ}$  (RH534) strains grown in complex PYE media. The cell length was measured by using MicrobeTracker software (Sliusarenko et al, 2011). The mean cell size  $\pm$  standard deviation (in  $\mu\text{m}$ ) of the different strains is indicated in brackets.

**B** Phase contrast imaging of wild-type (RH50),  $\Delta\text{gdhZ}$  (RH534), *ftsZ<sub>E79K</sub>* (NR6102), and *ftsZ<sub>E79K</sub> $\Delta\text{gdhZ}$*  (RH1329) strains, showing that combination of *ftsZ<sub>E79K</sub>* with  $\Delta\text{gdhZ}$  leads to a conspicuous filamentation. Scale bar, 5  $\mu\text{m}$ .

**C** Expression of *ftsZ-yfp* suppresses  $\Delta\text{gdhZ}$  cell division defect over time. Wild-type (RH53) and  $\Delta\text{gdhZ}$  (RH853) cells bearing an additional copy of *ftsZ* fused to *yfp* at the *vanA* locus (*P<sub>vanA</sub>::ftsZ-yfp*) were grown in PYE and imaged at different timepoints following induction of *ftsZ-yfp* expression with 0.5 mM vanillate. Scale bar, 5  $\mu\text{m}$ .

**D** Immunoblot of FtsZ and MreB steady-state levels in wild-type and  $\Delta\text{gdhZ}$  cell lysates showing that both strains have similar amount of FtsZ proteins. Protein extracts were prepared from wild-type (RH50) and  $\Delta\text{gdhZ}$  (RH534) strains, and twofold serial dilutions of cell lysates were separated on SDS-PAGE. The relative abundance of FtsZ and MreB intensities was quantified using ImageJ software, normalized according to the dilution factor. FtsZ levels were finally normalized according to MreB (FtsZ/MreB 100% in wild-type versus 103% in  $\Delta\text{gdhZ}$ ).

**E** Overexpression of *gdhZ* leads to cell filamentation.  $\Delta\text{gdhZ}$  cells expressing a *venus-gdhZ* fusion from *P<sub>xyIX</sub>* at the *xyIX* locus (RH740) were grown in PYE and imaged at different timepoints following induction of *venus-gdhZ* expression with 0.1% xylose. Scale bar, 5  $\mu\text{m}$ .

**F** Immunoblot of GdhZ and MreB showing levels of Venus-GdhZ increased over time in cells overexpressing *venus-gdhZ*. Proteins extracts were prepared from  $\Delta\text{gdhZ}$  *P<sub>xyIX</sub>::venus-gdhZ* (RH740) strain at the indicated timepoints after xylose induction and separated on SDS-PAGE. The level of GdhZ-GFP in strain RH602 was used as a control.

Source data are available online for this figure.

to ~85 min for the wild-type strain (Supplementary Fig S1). In addition, the proportion of late predivisional (constricting) cells, that is, predivisional cells with a visible ongoing constriction, was significantly ( $P < 0.001$ ) higher in  $\Delta gdhZ$  (~25%) than in wild-type (~10%). Surprisingly,  $\Delta gdhZ$  phenotypes were rescued when glucose, xylose, or alanine was added to PYE or used as the sole carbon source in synthetic media (Supplementary Fig S1 and data not shown). None of these carbon sources does require GDH activity to be catabolized *in vivo*. In contrast, amino acids feeding the Krebs cycle thanks to GdhZ activity (i.e. glutamate, histidine, proline, arginine, and glutamine; Fig 1B) did suppress neither growth nor cell division defects of  $\Delta gdhZ$  (data not shown). These results indicate that GdhZ might regulate cell division according to the carbon source used and that GDH activity might be essential for this regulation.

As the proportion of late predivisional cells was abnormally high in the  $\Delta gdhZ$  strain, we asked whether the deletion of *gdhZ* could specifically affect the G2 phase of the cell cycle. Flow cytometry analyses of the DNA content over the cell cycle showed that G1 and S phases were similar in both wild-type and  $\Delta gdhZ$  strains (Supplementary Fig S2). Likewise, the timing of localization of the G1-to-S transition markers MipZ-CFP (Thanbichler & Shapiro, 2006) and StpX-GFP (Hughes *et al*, 2010, 2013) was not affected in the  $\Delta gdhZ$  cells, supporting that GdhZ does regulate neither the G1 phase nor the transition to the S phase (Supplementary Fig S2). In contrast, the time spent at the division site by the late cell division marker TipN-GFP (Huitema *et al*, 2006; Lam *et al*, 2006; Goley *et al*, 2011) was prolonged in  $\Delta gdhZ$  cells (~60 min) in comparison with wild-type cells (~15 min). These observations are consistent with the high number of predivisional (constricting) cells observed in a  $\Delta gdhZ$  population and further support a role for GdhZ in cell division. In the same line, combination of  $\Delta gdhZ$  with *ftsZ<sub>E79K</sub>* resulted in an exacerbated filamentation (Fig 2B). Initially isolated as a mutant that tolerates *kidO* overexpression, *ftsZ<sub>E79K</sub>* is still able to sustain cell division despite a twofold reduced GTPase activity (Radhakrishnan *et al*, 2010). On the contrary, expression of a second copy of *ftsZ* fused to *yfp* from an inducible promoter (*P<sub>vanA</sub>::ftsZ-yfp*) suppressed the cell size heterogeneity (Fig 2C and Supplementary Fig S3A), but not the growth defect of  $\Delta gdhZ$  (Supplementary Fig S3B). Indeed, after 3 h of induction with vanillate, the average cell size of  $\Delta gdhZ$  cells varied from  $2.0 \pm 1.5 \mu\text{m}$  to  $2.5 \pm 0.8 \mu\text{m}$ , a distribution similar to a wild-type population grown in the same conditions ( $2.7 \pm 0.7 \mu\text{m}$ ). This result prompted us to check whether intracellular level of FtsZ decreased in the absence of *gdhZ*. Quantification of immunoblot analyses revealed that FtsZ levels in  $\Delta gdhZ$  cells corresponded to 103% of wild-type FtsZ levels (Fig 2D), suggesting that GdhZ does not control FtsZ levels but rather its dynamics. Finally, overexpression of *gdhZ* fused to *venus* from the inducible *P<sub>xytX</sub>* promoter (*P<sub>xytX</sub>::venus-gdhZ*) gave rise to cell filamentation upon addition of xylose (Fig 2E and F), without seriously interfering with cell growth (Supplementary Fig S1E and F).

Altogether these results suggest that GdhZ is a metabolic regulator controlling late steps of cell division according to the carbon source catabolized by *C. crescentus*.

### GdhZ regulates FtsZ dynamics *in vivo*

Since *gdhZ* is required for efficient cell division, we tested whether GdhZ controls FtsZ dynamics *in vivo* by monitoring the distribution

of FtsZ-YFP in wild-type and  $\Delta gdhZ$  cells (Fig 3A). By plotting FtsZ-YFP intensity profile along the cell length, we did not detect any FtsZ misplacement in  $\Delta gdhZ$  cells (Fig 3A). In contrast, we found that the proportion of cells with a detectable medial Z-ring was significantly ( $P < 0.001$ ) higher in  $\Delta gdhZ$  ( $87.5 \pm 1.8\%$ ;  $n = 672$ ) than in the wild-type strain ( $70.4 \pm 5.4\%$ ;  $n = 716$ ). Similar observations were made with MreB, which is recruited very early at the Z-ring (Goley *et al*, 2011), since  $90.0 \pm 2.6\%$  ( $n = 937$ ) of  $\Delta gdhZ$  cells displayed a midcell localization for GFP-MreB versus  $76.3 \pm 3.5\%$  ( $n = 635$ ) for wild-type cells ( $P < 0.001$ ). These results suggest that FtsZ could be prematurely recruited at the midcell in small G1 swarmer cells in the absence of *gdhZ*. To test that, we determined the localization of FtsZ-YFP in wild-type and  $\Delta gdhZ$  small G1 swarmer cells ( $\leq 2 \mu\text{m}$ ). As expected, FtsZ-YFP was mostly observed at a pole ( $75.7\%$ ,  $n = 70$ ) and occasionally at midcell ( $7.1\%$ ,  $n = 70$ ) of wild-type cells  $\leq 2 \mu\text{m}$ . In  $\Delta gdhZ$  cells  $\leq 2 \mu\text{m}$ , FtsZ-YFP localized more often at a midcell position ( $24.7\%$ ,  $n = 121$ ), and less frequently at a pole ( $38.8\%$ ,  $n = 121$ ). Thus, FtsZ is prematurely assembled as a Z-ring in  $\Delta gdhZ$  G1 swarmer cells. As the expression of *ftsZ-yfp* suppresses  $\Delta gdhZ$  cell division defects (Fig 2C), we sought to use a strain expressing *gfp-fzIC* from the inducible *xytX* promoter (*P<sub>xytX</sub>::gfp-fzIC*) to monitor FtsZ localization throughout the cell cycle. Indeed, GFP-FzIC not only mirrors FtsZ localization (Goley *et al*, 2011), but most of all, its expression does not mitigate  $\Delta gdhZ$  phenotypes (data not shown). Time-lapse experiments revealed that GFP-FzIC failed to disappear from the contracting Z-ring in late predivisional cells, but also relocalized at the midcell of future daughter cells prior to the completion of cell division in  $\Delta gdhZ$  cells (Fig 3B).

These data indicate that GdhZ inhibits the formation and/or stability of the Z-ring, presumably in G2 phase to stimulate its disassembly and in G1 phase to prevent the assembly of a new Z-ring before the constricting one is disassembled.

### GdhZ colocalizes with FtsZ at midcell

To further characterize the role of GdhZ in cell division control, we determined its subcellular localization in strains expressing either *gdhZ-gfp* at the native *gdhZ* locus or *venus-gdhZ* from the inducible *P<sub>xytX</sub>* promoter. Both GdhZ-GFP and Venus-GdhZ fusions accumulated at a medial position (Fig 3C). Interestingly, GdhZ-GFP no longer localized at midcell when glucose or xylose was added to the culture medium (data not shown). Let's remind that these two carbon sources suppressed cell growth and division defects of  $\Delta gdhZ$  cells (Supplementary Fig S1 and data not shown). Coexpressing *gdhZ-gfp* and *ftsZ-mcherry* from the inducible *P<sub>xytX</sub>* promoter confirmed that GdhZ-GFP fluorescence signal was enriched at or near the Z-ring (i.e. where FtsZ-mCherry localized) in more than 70% ( $n = 437$ ) of cells displaying a GdhZ-GFP signal (Fig 3D). Similar results were obtained with GdhZ-GFP and mCherry-FzIC, since both proteins colocalized in ~65% of cells (Supplementary Fig S4A). In addition, demographic representations of GdhZ-GFP and FtsZ-mCherry signals allowed us to monitor the dynamic localization of both proteins along the cell cycle from a heterogeneous population. As expected, FtsZ-mCherry was found at one pole of small G1 swarmer cells before being relocated at a medial position in larger cells (Figs 1A and 3E). In contrast, GdhZ-GFP was not localized at one pole in small G1 swarmer cells (Fig 3E), but started to accumulate at midcell in larger cells, slightly

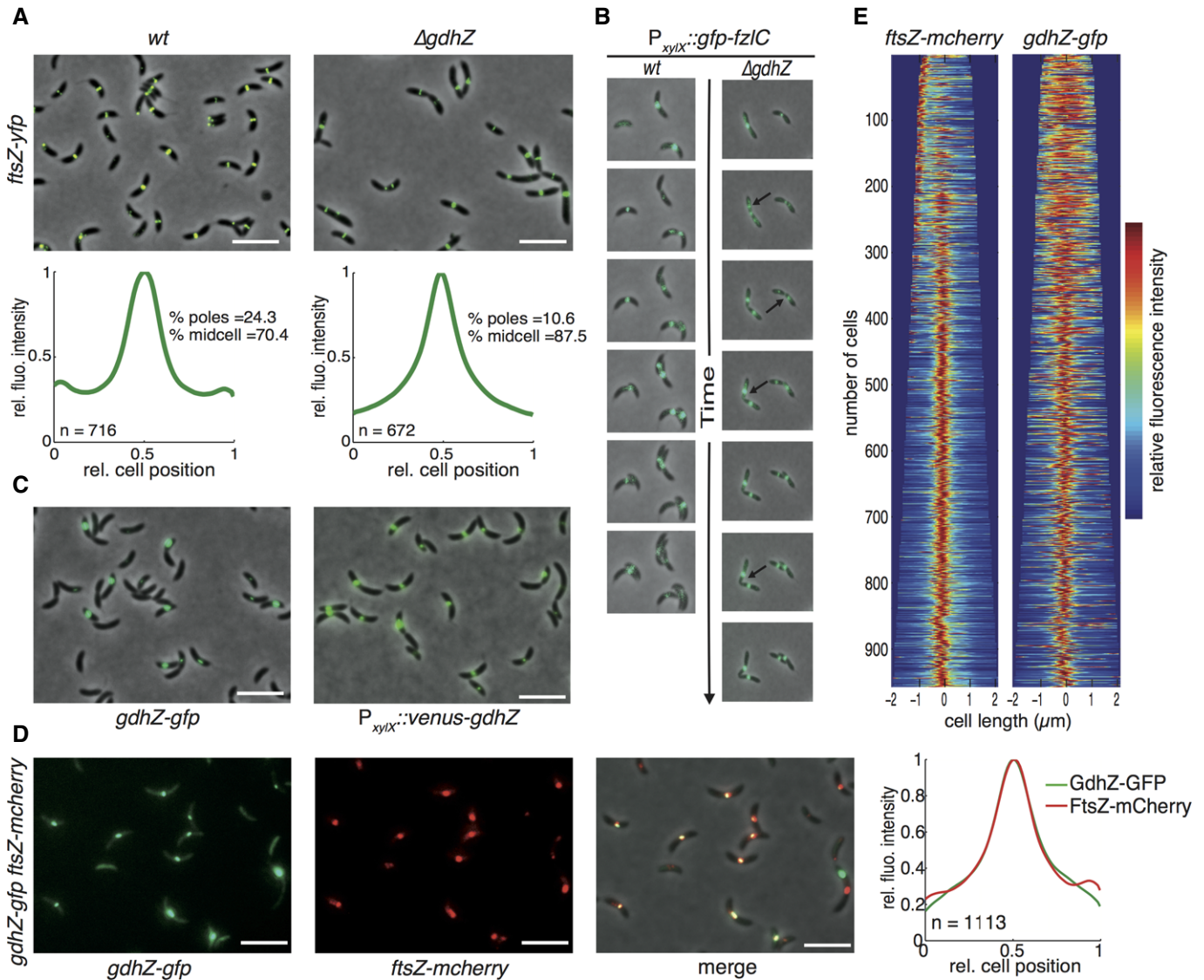


**Figure 3. GdhZ regulates Z-ring dynamics *in vivo*.**

- A** Localization of FtsZ-YFP determined by phase contrast and fluorescence microscopy of wild-type (RH53) and  $\Delta$ *gdhZ* (RH853) cells expressing *ftsZ-yfp* from  $P_{vanA}$  at the *vanA* locus. Expression of *ftsZ-yfp* was induced by adding 0.5 mM vanillate to the cultures 1 h before imaging. Scale bar, 5  $\mu$ m. FtsZ-YFP signal from wild-type and  $\Delta$ *gdhZ* cells was plotted according to the cell length. "0" and "1" correspond to the poles, and "0.5" to the midcell position.
- B** Time-lapse fluorescence microscopy of wild-type (RH1733) and  $\Delta$ *gdhZ* (RH1734) cells harboring  $P_{xyiX}::gfp-fzIC$ , showing the dynamic localization of GFP-FzIC throughout the cell cycle. Cells were grown in PYE, and xylose was added 1 h before spotting cells on PYE agarose pad. Each picture was taken every 35 min. Arrows point to premature recruitment of GFP-FzIC at future division sites in daughter cells prior to the completion of cell division.
- C** Localization of GdhZ-GFP or Venus-GdhZ, determined by phase contrast and fluorescence microscopy of *gdhZ-gfp* (RH602) or  $\Delta$ *gdhZ*  $P_{xyiX}::venus-gdhZ$  (RH740). Expression of *venus-gdhZ* induced by adding 0.05% xylose was added to the cultures 30 min before imaging. Scale bar, 5  $\mu$ m.
- D** Colocalization of GdhZ-GFP with FtsZ-mCherry, determined by phase contrast and fluorescence microscopy of *gdhZ-gfp*  $P_{xyiX}::ftsZ-mcherry$  (RH967). The expression of *ftsZ-mcherry* was induced by adding 0.1% xylose to the cultures 30 min before imaging. Scale bar, 5  $\mu$ m. GdhZ-GFP (green) and FtsZ-mCherry (red) signals from *gdhZ-gfp*  $P_{xyiX}::ftsZ-mcherry$  cells were plotted according to the cell length. "0" and "1" correspond to the poles, and "0.5" to the midcell position.
- E** Demographic representation of FtsZ-mCherry and GdhZ-GFP fluorescent patterns (n = 957). The signal intensity in each cell is represented by a color code, from dark blue (low intensity) to red (high intensity). "0" corresponds to the midcell position.

after the Z-ring was assembled at the division site (Fig 3E). This result suggests that GdhZ could be recruited at midcell directly by FtsZ. To test that, the localization of GdhZ-Venus and mCherry-FzIC was assessed in a strain where the only copy of *ftsZ* was under the control of the inducible  $P_{xyiX}$  promoter. After 3 h of xylose depletion,

GdhZ-Venus still displayed a discrete localization ( $\leq 1$  focus per cell), while mCherry-FzIC was mostly diffuse in the cytoplasm (Supplementary Fig S4B and C). However, GdhZ-Venus no longer concentrated at midcell (Supplementary Fig S4D), suggesting that GdhZ midcell recruitment relies on FtsZ.

These observations suggest that GdhZ accumulates at the division site in a FtsZ-dependent manner very likely to stimulate Z-ring disassembly in late predivisional cells.

### GdhZ modulates FtsZ dynamics *in vitro*

Our observations so far implicate GdhZ as a negative regulator of the Z-ring. We thus tested the ability of GdhZ to modulate FtsZ dynamics *in vitro*. For this purpose, we purified native GdhZ and monitored its activity (oxidative deamination) by following NADH production at 340 nm. The reaction was defined as a function of the concentration of NAD<sup>+</sup> or glutamate (Supplementary Fig S5). The NAD<sup>+</sup> saturation curve followed a Michaelis–Menten kinetics, yielding a  $K_m$  value of 0.038 mM (Supplementary Fig S5A). In contrast, the glutamate saturation curve was sigmoidal, and a Hill plot established a  $S_{0.5}$  of 42.5 mM with an interaction coefficient ( $n$ ) of 1.6, indicating a positive cooperativity in glutamate binding (Supplementary Fig S5B).

Since purified GdhZ was active *in vitro*, we then measured the intrinsic GTPase activity of FtsZ and visualized the formation of FtsZ ordered structures (protofilaments and bundles) by negative-stain electron microscopy (EM), in the presence or absence of GdhZ. First, the addition of increasing concentration of GdhZ did not substantially affect the GTPase activity of FtsZ, with only a slight increase (~30%) in GTP hydrolysis at a 2:1 GdhZ:FtsZ molar ratio (Fig 4A). In contrast, the addition of GdhZ together with its substrates (NAD<sup>+</sup> and glutamate) strongly stimulated the GTPase activity of FtsZ in a dose-dependent manner (Fig 4B) (~4.5-fold increase at 2:1 GdhZ:FtsZ ratios). Interestingly, the presence of only one of the substrates (NAD<sup>+</sup> or glutamate) was sufficient for GdhZ to stimulate the GTPase activity of FtsZ (Supplementary Fig S6A), suggesting that a conformational change of GdhZ induced by substrate binding allows GdhZ to interfere with FtsZ dynamics *in vitro*. Then, we examined the effect of GdhZ on FtsZ ultrastructures by EM. In agreement with earlier studies, in the presence of GTP, FtsZ assembled into straight protofilaments that can associate into bundles (Fig 4C). Consistent with the above results, FtsZ structures were still visible in the presence of GdhZ alone (Fig 4D), but barely detectable when GdhZ and its substrates were included in the reactions, with only a few short protofilaments observed at a 1:1 GdhZ:FtsZ ratio (Fig 4E). Note that GdhZ also self-assembles into higher ordered structures in a concentration-dependent manner (F. Beaufay and R. Hallez, unpublished results), which affected the negative-staining contrast. Importantly, neither substrates nor products of GDH reaction (NAD(H), glutamate, ammonium, or  $\alpha$ -ketoglutarate) did, on themselves, neither stimulate the GTPase activity nor influence the polymeric structures of FtsZ in the tested conditions (Fig 4B and data not shown). Likewise, the dynamics of FtsZ was not affected by the unrelated bovine L-glutamic dehydrogenase GdhA with its substrates (Supplementary Fig S6B and E). Finally, we found that FtsZ<sub>E79K</sub>, which displays a twofold reduced GTPase activity compared to wild-type FtsZ, was still fully sensitive to active GdhZ (Supplementary Fig S6C and F). The GTPase activity of FtsZ<sub>E79K</sub> was indeed strongly stimulated by active GdhZ (~ninefold at 2:1 GdhZ:FtsZ<sub>E79K</sub> ratio).

On the basis of these *in vitro* data, we propose that catalytically active GdhZ very likely disassembles FtsZ polymers by triggering the GTPase activity of FtsZ.

### GdhZ activity is required to control the cell division process

The fact that GdhZ substrates are required *in vitro* for GdhZ to stimulate the GTPase activity of FtsZ prompted us to investigate the effect of a catalytically inactive mutant of GdhZ (GdhZ<sub>K837A</sub>) on cell division. GdhZ<sub>K837A</sub> was stable *in vivo* and purified GdhZ<sub>K837A</sub> displayed no detectable GDH activity *in vitro* in contrast to wild-type GdhZ (Supplementary Fig S7A). We found that *gdhZ*<sub>K837A</sub> phenocopied  $\Delta$ *gdhZ* in terms of (i) growth and cell division defects (Supplementary Figs S1, S7B and S7C), (ii) synthetic interaction with *ftsZ*<sub>E79K</sub> (Supplementary Fig S7C), and (iii) premature GFP-FzIC recruitment at midcell (Supplementary Fig S7D and data not shown). In addition, GdhZ<sub>K837A</sub> did not affect FtsZ dynamics (Supplementary Fig S6D and E), even if it could still pull down FtsZ (Supplementary Fig S7E).

These results further support the idea that GDH activity is strictly required for GdhZ to control cell division but not to mediate interaction with FtsZ.

### GdhZ abundance oscillates over the cell cycle

The abundance of FtsZ and several of its regulators (FtsA, FzIA, FtsQ, or KidO) was previously shown to oscillate during the cell cycle in order to coordinate cell division events (Kelly *et al*, 1998; Martin *et al*, 2004; Goley *et al*, 2010; Radhakrishnan *et al*, 2010). To determine whether GdhZ is also cell-cycle-regulated, we monitored GdhZ abundance over the cell cycle in a synchronized population of *Caulobacter* cells in which the native copy of *gdhZ* was replaced by a functional 3FLAG-*gdhZ* fusion. As illustrated in Fig 5A, 3FLAG-GdhZ oscillated throughout the cell cycle, reaching the highest level in swarmer and late predivisional cells and the lowest level in stalked cells. This cell cycle fluctuation was also observed in the wild-type strain using polyclonal anti-GdhZ antibodies (Fig 5B). Thus, GdhZ starts to disappear in differentiating stalked cells (i.e. when the Z-ring is built up) and reappears in late predivisional cells (i.e. when the Z-ring starts to be disassembled) (Fig 5A and Supplementary Fig S8A).

Several evidence support that GdhZ might be subjected to a cell cycle-dependent proteolysis. First, adding a 3FLAG tag or GFP at GdhZ C-terminus (GdhZ-3FLAG or GdhZ-GFP) or substituting the last two alanine residues by two aspartate residues (GdhZ<sub>AA::DD</sub>) completely abrogated oscillation (Fig 5C and Supplementary Fig S8B and data not shown). This is reminiscent of that seen for other cell-cycle-regulated proteins degraded by the ClpXP protease (Domian *et al*, 1997; Radhakrishnan *et al*, 2010; Abel *et al*, 2011). Indeed, GdhZ has a C-terminal end homologous to the proteolytic SsrA peptide tag (Fig 5D) known to deliver substrates to ClpXP. Masking or mutating this conserved motif could block proteolysis as it is the case for CtrA or KidO (Domian *et al*, 1997; Radhakrishnan *et al*, 2010; Abel *et al*, 2011). Second, the steady-state level of GdhZ increased in the absence of the ClpP peptidase subunits (Fig 5E). Third, 3FLAG-GdhZ did not oscillate anymore in mutants (*ΔcpdR*, *ΔrcdA*, and *ΔpopA*) unable to degrade ClpXP-dependent substrates (Supplementary Fig S8C) (Inieta *et al*, 2006; McGrath *et al*, 2006; Duerig *et al*, 2009). Together these results suggest that, similar to KidO, GdhZ undergoes a ClpXP-dependent degradation throughout the cell cycle.

The reappearance of GdhZ in late predivisional cells could be due to the transcriptional activation of *gdhZ* by the response

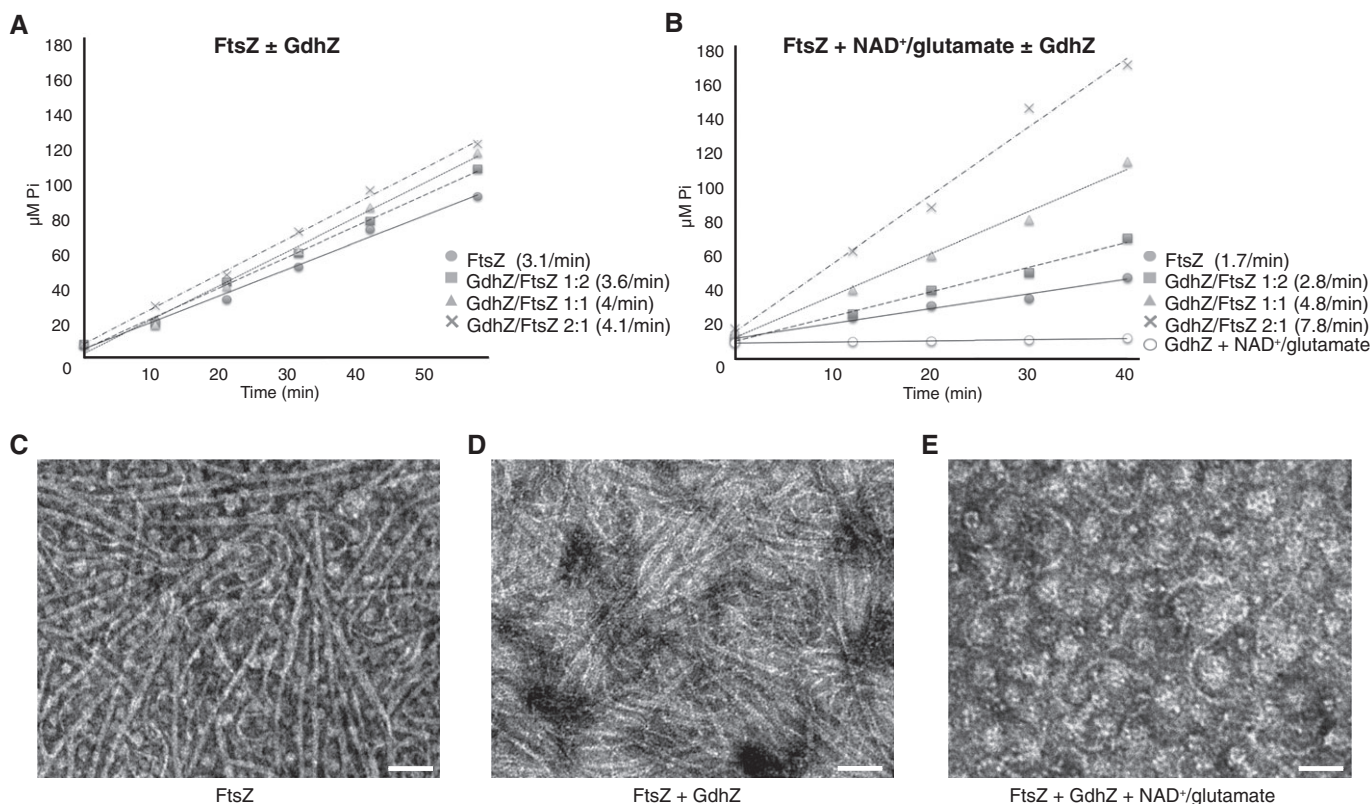


**Figure 4. Active GdhZ promotes FtsZ's GTPase activity *in vitro* leading to filaments disassembly.**

**A** Inorganic phosphate (P<sub>i</sub>) release over time by FtsZ (0.5 μM) incubated with 1 mM GTP in the presence of 0, 0.25, 0.5, or 1 μM GdhZ, respectively. The rates of GTPase (P<sub>i</sub> released per FtsZ molecule per min) are indicated for each condition.

**B** Stimulation of FtsZ's GTPase activity with active GdhZ. Inorganic phosphate (P<sub>i</sub>) release over time by FtsZ (0.5 μM) incubated with 1 mM GTP, 100 mM glutamate, 5 mM NAD<sup>+</sup> in the presence of 0, 0.25, 0.5, or 1 μM GdhZ, respectively. The rates of GTPase (P<sub>i</sub> molecules released per FtsZ per min) are indicated for each condition. Note that GdhZ with its substrates (100 mM glutamate, 5 mM NAD<sup>+</sup>) does not display any detectable GTPase activity on itself.

**C–E** Negative-stain electron microscopy of FtsZ (0.5 μM) incubated with 1 mM GTP in the absence (c) or presence of 0.5 μM GdhZ alone (d) or together with 100 mM glutamate and 5 mM NAD<sup>+</sup> (e). Scale bar, 100 nm.

Source data are available online for this figure.

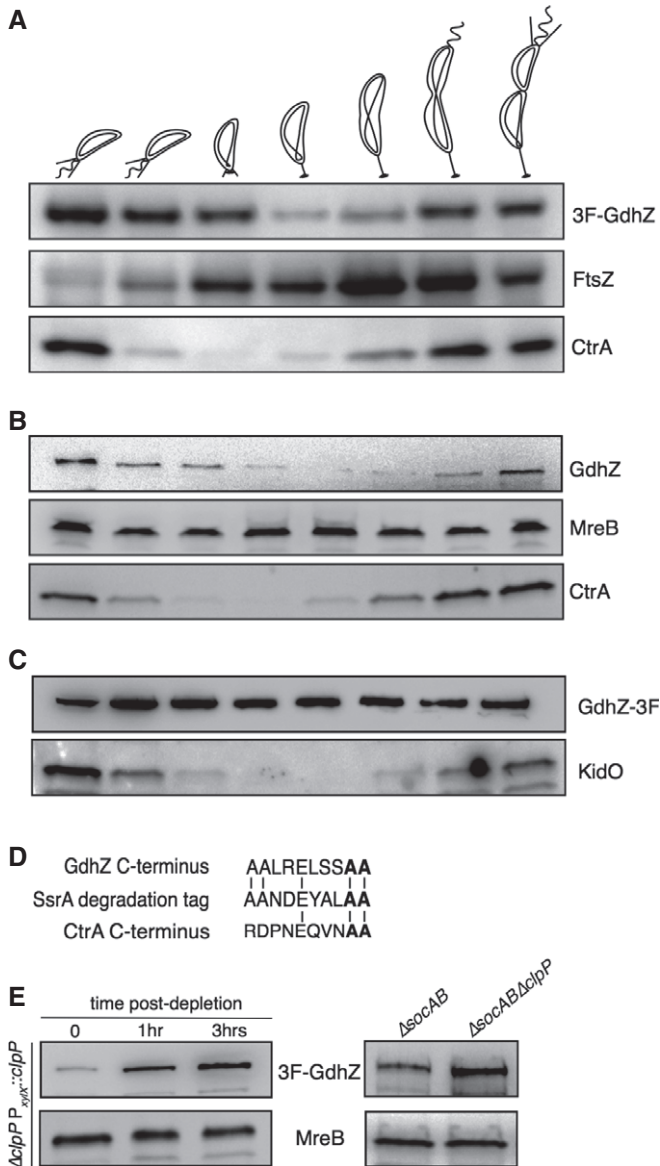
regulator CtrA, as described for KidO (Radhakrishnan *et al.*, 2010). Indeed, CtrA, known to modulate the transcription of cell-cycle-regulated genes (Laub *et al.*, 2000), has recently been shown to tightly bind the promoter region of *gdhZ* ( $P_{gdhZ}$ ) (Fumeaux *et al.*, 2014). To test this hypothesis, the transcription of *gdhZ* was monitored with a  $P_{gdhZ}::lacZ$  transcriptional fusion in strains in which CtrA is either underactivated ( $\Delta pleC$ ) or overactivated ( $\Delta divJ$  or  $divK^{cs}$ ) (Supplementary Fig S9A). We found that  $P_{gdhZ}$  activity was reduced by ~25% in  $\Delta pleC$  cells and increased by ~25% in  $\Delta divJ$  or  $divK^{cs}$  cells in comparison with wild-type cells (Supplementary Fig S9B). Accordingly, the steady-state level of GdhZ was increased in  $divK^{cs}$  cells and decreased in a strain expressing a thermosensitive loss-of-function mutant of *ctrA* (Supplementary Fig S9C). These results strongly suggest that CtrA~P directly activates the transcription of *gdhZ*.

Overall, we propose that GdhZ uses the same regulatory network as KidO to oscillate throughout the cell cycle, very likely to limit its abundance during the S phase of the cell cycle, that is, when the Z-ring has to be built up. Taken this into consideration, the localization of GdhZ-GFP at the midcell during S phase (stalked and early

predivisive cells), depicted on Fig 3E, very likely resulted from the stabilization of the fusion protein. Therefore, we can postulate that GdhZ is recruited to the division site in late predivisive cells, very likely to trigger Z-ring disassembly.

#### KidO inhibits lateral interactions between FtsZ protofilaments

By inhibiting Z-ring formation in swarmer cells (G1) and stimulating Z-ring disassembly in late predivisive cells (G2), GdhZ would play a role similar to the one already proposed for KidO (Radhakrishnan *et al.*, 2010). However, the exact mechanism by which KidO, once bound to NAD(H), interferes with FtsZ remains unknown. To address this question, KidO was purified and its effect on the polymerization of FtsZ was measured *in vitro*. In contrast to GdhZ with its substrates, KidO alone (Fig 6A) or with its cofactor (NAD<sup>+</sup> or NADH, Fig 6B) did not substantially affect the GTPase activity of FtsZ. At a 2:1 KidO:FtsZ ratio, KidO slightly increases the GTP hydrolysis rate of FtsZ (~30%) in the presence of either NADH or NAD<sup>+</sup> (compare Figs 6B and 4B). However, EM analyses revealed that, in the presence of NADH but not NAD<sup>+</sup>, KidO drastically



reduced FtsZ bundling without interfering with single protofilaments (Fig 6D). These results suggest that KidO bound to NADH hampers lateral interactions between FtsZ protofilaments rather than stimulating FtsZ's GTPase activity. This observation is consistent with the drastic increase of bundling capacity that we observed for the KidO-resistant mutant FtsZ<sub>E79K</sub> (Supplementary Fig S6F). In comparison with wild-type FtsZ, FtsZ<sub>E79K</sub> assembled *in vitro* into larger and longer polymeric structures (compare Supplementary Fig S6E and F), very likely by increasing lateral interactions between FtsZ protofilaments. In that case, the reduced GTPase activity of FtsZ<sub>E79K</sub> would therefore be an indirect consequence of the increased bundling. On the other hand, the fact that GdhZ and KidO use different molecular mechanisms to control cell division explains the sensitivity of the KidO-resistant mutant FtsZ<sub>E79K</sub> to active GdhZ (Supplementary Fig S6C) as well as the synthetic interactions observed between *ftsZ*<sub>E79K</sub> and  $\Delta gdhZ$  or *gdhZ*<sub>K837A</sub> (Fig 2B and Supplementary Fig S7C). The robust Z-rings formed *in vivo* by

**Figure 5. The ClpXP protease is responsible for the cell cycle oscillation of GdhZ.**

- A** Immunoblotting of protein samples extracted from synchronized 3FLAG-*gdhZ* (RH743) cells to follow 3FLAG-GdhZ, FtsZ and CtrA abundance throughout the cell cycle.
- B** Immunoblotting of protein samples extracted from synchronized wild-type (RH50) cells to follow GdhZ and CtrA abundance throughout the cell cycle.
- C** Immunoblotting of protein samples extracted from synchronized *gdhZ*-3FLAG (RH728) cells to follow GdhZ-3FLAG and KidO abundance throughout the cell cycle.
- D** Alignment of the C-terminal extremity of GdhZ, CtrA and SsrA tag. The last two hydrophobic amino acids (Ala-Ala) are essential for degradation of substrates by ClpXP.
- E** Steady-state levels 3FLAG-GdhZ and MreB in *clpP* depletion (RH991, left panel) or deletion (RH1672 and RH1675, right panel) strains revealed by immunoblots (level of 3FLAG-GdhZ increased ~threefold and ~twofold, respectively).  $\Delta clpP$   $P_{xyk}::clpP$  3FLAG-*gdhZ* cells were grown in PYE supplemented with 0.1% xylose to mid-exponential phase and then washed and resuspended in PYE without xylose. Deletion *clpP* is known to be viable in strain deleted for the toxin-antitoxin system *socAB* (Aakre et al, 2013).  $\Delta socAB$  (RH1672) and  $\Delta socAB \Delta clpP$  (RH1675) cells were grown in PYE to mid-exponential phase.

Source data are available online for this figure.

FtsZ<sub>E79K</sub> could not be properly disassembled without the GdhZ-dependent stimulation of FtsZ GTPase activity.

Thus, GdhZ and KidO might control FtsZ by using different and complementary mechanisms to trigger Z-ring disassembly.

#### KidO and GdhZ work in synergy to trigger Z-ring disassembly

As both GdhZ and KidO (i) inhibit Z-ring assembly/stability in swarmer and late predivisional cells, (ii) share the same regulatory network to oscillate throughout the cell cycle, and (iii) use NAD(H) as a cofactor, we wondered whether KidO and GdhZ could act in coordination to control Z-ring dynamics. To test this idea, we created a *C. crescentus* strain in which both proteins were stabilized, that is, not anymore proteolyzed by ClpXP. If both proteins disassemble FtsZ polymers, we predict that their presence at the onset of the S phase would interfere with Z-ring formation. As expected, this strain (*gdhZ-gfp kidO*<sub>AA::DD</sub>) exhibited a strong filamentation, much stronger than the strain expressing either *gdhZ-gfp* or *kidO*<sub>AA::DD</sub> (Supplementary Fig S10A and B). Interestingly, this filamentation was completely abolished when glucose was added to the medium (data not shown), supporting that GdhZ and/or KidO are controlled by nutrient availability. We then tested whether KidO could enhance the effect of active GdhZ on the GTPase activity of FtsZ. As shown on Fig 6C, the presence of KidO increased the stimulation of FtsZ GTPase activity by active GdhZ (~30%) although NADH was only generated by GDH activity. The NADH produced by GdhZ could therefore be directly delivered to KidO to disassemble FtsZ bundles. In support of this idea, GdhZ and KidO co-purified in a pull-down assay suggesting that both proteins are part of the same complex (Supplementary Fig S10C).

These results suggest that GdhZ and KidO act in synergy to stimulate depolymerization of the Z-ring, KidO-NADH dissociating FtsZ bundles and active GdhZ stimulating GTPase activity of newly available FtsZ protofilaments.

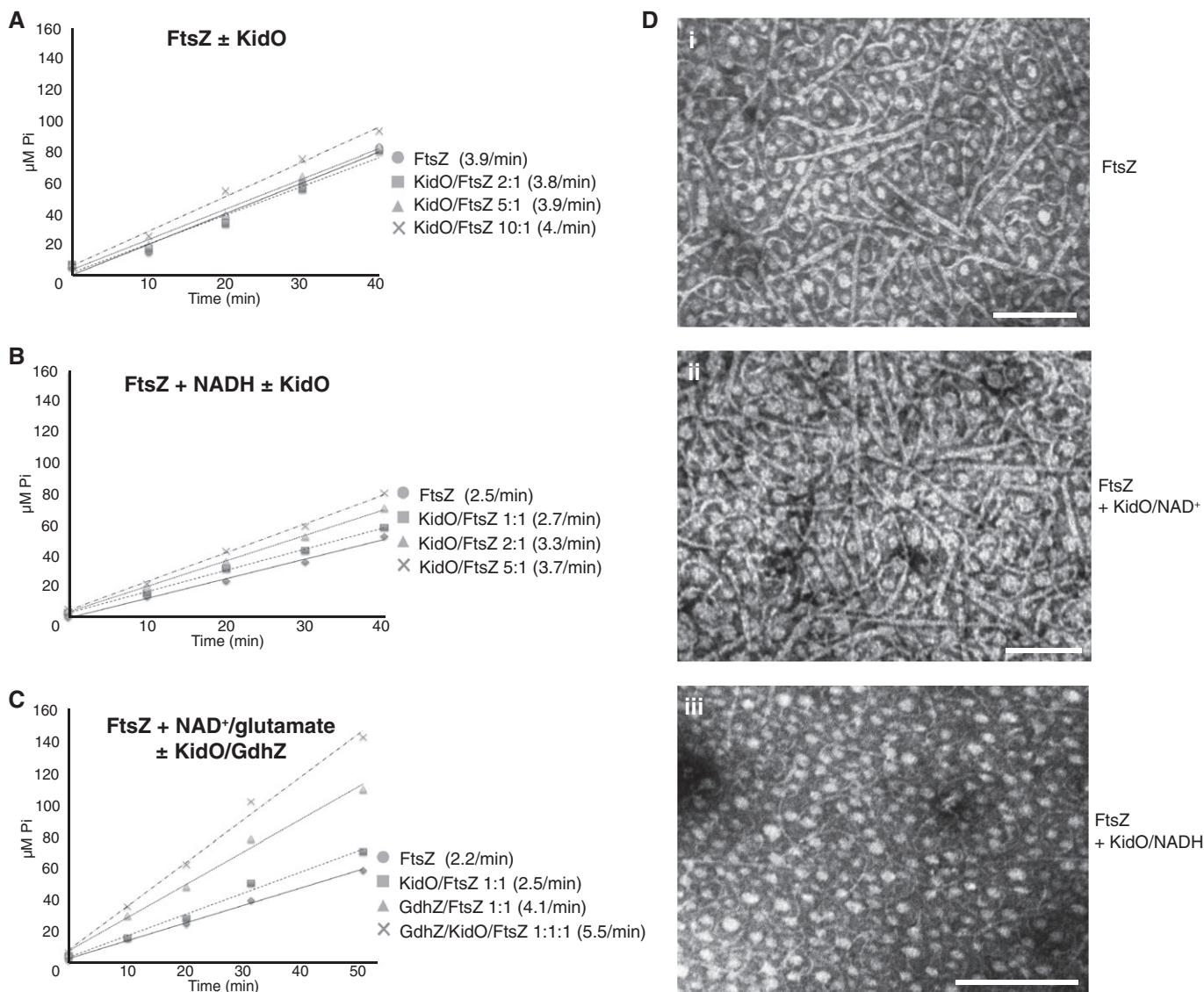


**Figure 6. NADH-bound KidO prevents lateral interactions between FtsZ protofilaments.**

A Inorganic phosphate ( $P_i$ ) release over time by FtsZ (0.5  $\mu$ M) incubated with 1 mM GTP in the presence of 0, 1, 2.5, or 5  $\mu$ M KidO, respectively. The rates of GTPase ( $P_i$  released per FtsZ molecule per min) are indicated for each condition.

B KidO does not strongly stimulate GTPase activity of FtsZ in the presence of NADH. Inorganic phosphate ( $P_i$ ) release over time by FtsZ (0.5  $\mu$ M) incubated with 1 mM GTP, 5 mM NADH in the presence of 0, 0.5, 1, or 2.5  $\mu$ M KidO, respectively. The rates of GTPase ( $P_i$  molecules released per FtsZ per min) are indicated for each condition. Similar results were obtained when NAD<sup>+</sup> was used instead of NADH (data not shown).

C KidO enhances the effect of GdhZ on the GTPase activity of FtsZ. Inorganic phosphate ( $P_i$ ) release over time by FtsZ (0.5  $\mu$ M) incubated with 1 mM GTP, 100 mM glutamate, 5 mM NAD<sup>+</sup>, in the absence or presence of 0.5  $\mu$ M KidO, or 0.5  $\mu$ M GdhZ, or both 0.5  $\mu$ M KidO and 0.5  $\mu$ M GdhZ. The rates of GTPase ( $P_i$  molecules released per FtsZ per min) are indicated for each condition.

D Negative-stain electron microscopy of FtsZ (0.5  $\mu$ M) incubated with 1 mM GTP, in the presence of 1  $\mu$ M KidO without NAD(H) (i), or with 5 mM NAD<sup>+</sup> (ii) or 5 mM NADH (iii). Scale bar, 200 nm. Note that neither NADH nor NAD<sup>+</sup> does affect FtsZ polymerization.

Source data are available online for this figure.

## Discussion

Here, we found that the NAD-dependent glutamate dehydrogenase GdhZ coordinates metabolism with cell division in *C. crescentus*. GdhZ directly stimulates the GTPase activity of FtsZ, and this regulation requires GdhZ catalytic activity. The central position of GDH reaction between the TCA and nitrogen cycles makes GdhZ an

excellent candidate and as a metabolic regulator of the cell cycle (Figs 1B and 7). So far, the best characterized bacterial metabolic regulators of cell division are UgtP in *Bacillus subtilis* and OpgH in *Escherichia coli*; both are glucosyltransferases using UDP-glucose as a substrate (Weart *et al.*, 2007; Hill *et al.*, 2013). These proteins coordinate growth with cell division to adapt cell size according to nutrient availability. In contrast to *C. crescentus*, *E. coli* and

*B. subtilis* can indeed adjust their cell size depending on their growth rate (Sargent, 1975; Campos *et al*, 2014). Similar to UgtP and OpgH, GdhZ directly interferes with FtsZ. However, in contrast to GdhZ, UgtP and OpgH do not require their substrates to inhibit FtsZ polymerization *in vitro*. The cell division control by UgtP or OpgH is rather driven by their steady-state levels, which, in turn, are determined by nutrient availability. In addition, GdhZ mainly stimulates the GTPase activity of FtsZ, while UgtP inhibits FtsZ single-filament formation and OpgH sequesters FtsZ monomers preventing them from assembly (Weart *et al*, 2007; Hill *et al*, 2013).

KidO is another metabolic regulator of cell division in *C. crescentus*, described to stimulate the disassembly of the Z-ring in a NAD(H)-dependent manner (Radhakrishnan *et al*, 2010), during the G1 and G2 phases of the cell cycle. We showed that GdhZ and KidO share the same regulatory network. First, ClpXP degrades both proteins at the G1-to-S transition, to ensure that they mainly disappear when the Z-ring needs to be assembled at the division site (early S phase). Second, the master regulator CtrA positively regulates the transcription of *gdhZ* and *kidO*, and this coregulation allows reaccumulation of both proteins in G2 phase to stimulate the rapid depolymerization of the Z-ring during cytokinesis (Fig 7). Change in NAD(H) levels during the cell cycle has been initially proposed to drive KidO-dependent cell division control (Radhakrishnan *et al*, 2010). Alternatively, GdhZ might directly deliver NADH to KidO in the vicinity of the Z-ring, through its catabolic

activity (Fig 7). This “substrate channeling-like” process (Schendel *et al*, 1988; Arentson *et al*, 2012; Dunn, 2012) would coordinate GdhZ and KidO activities on the Z-ring during the G2 phase of the cell cycle, in order to facilitate Z-ring disassembly and cytokinesis. Similar to KidO, GdhZ also prevents premature Z-ring formation during the G1 phase. Indeed, time-lapse experiments showed that  $\Delta$ *gdhZ* predivisional cells could assemble a new Z-ring at the division site of future daughter cells prior to the completion of cell division (Fig 3B). In addition, a  $\Delta$ *gdhZ* mutant gives birth to small swarmer progeny cells that have already built up a Z-ring (Fig 3A). On the basis of these observations, we propose a model (Fig 7) in which GdhZ and KidO coordinately prevent premature assembly of the Z-ring in G1 swarmer cells. Then, the ClpXP-dependent proteolysis of GdhZ and KidO at the G1-S transition allows the building of the Z-ring. Later in the cell cycle (G2 phase), both proteins reaccumulate to reach their maximal levels at the late predivisional stage of the cell cycle. At that time, KidO destabilizes lateral interactions between FtsZ protofilaments, thereby increasing filament sliding, while active GdhZ stimulates the GTPase activity of FtsZ to ensure that the Z-ring does not reach a too condensed state that could block cytokinesis (Szwedziak *et al*, 2014). The concomitant recruitment of two negative regulators of the Z-ring at the onset of the G2 phase could therefore be responsible for the 2-step motion of cytokinesis (first slow, then rapid) described for *C. crescentus* (Holden *et al*, 2014).

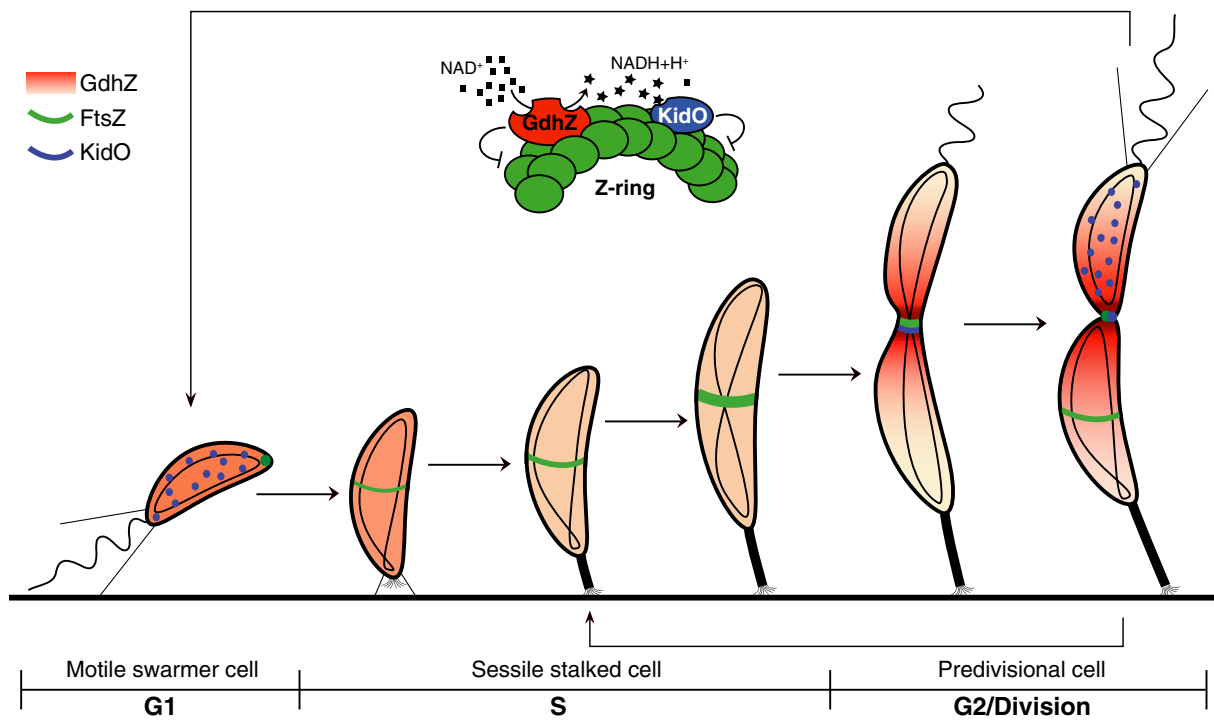


**Figure 7. Model for the coordination of cell division with metabolism through the concomitant and synergic action of GdhZ and KidO.**

GdhZ and KidO abundance oscillate throughout the cell cycle to reach maximal levels during G1 and G2 phases. Localization of GdhZ and KidO to the Z-ring allows both proteins to accumulate in the vicinity of the division site, at the constriction step. Each protein can, independently of each other, avoid premature Z-ring assembly in G1 swarmer cell and promote Z-ring disassembly in G2 predivisional cells. As being part of the same complex, we propose that GdhZ could locally provide KidO with NADH thanks to glutamate catabolism. This “substrate channeling-like” mechanism could enhance Z-ring disassembly. According to nutrient availability, the synergic action of both GdhZ and KidO could be responsible for the rapid constriction observed during G2 phase (Holden *et al*, 2014). In starving conditions, GdhZ and KidO would not stimulate constriction, therefore delaying cell division and preventing the release of the swarmer progeny cells without enough energy and nutrients to colonize new environments.

Although  $\Delta gdhZ$  cells spend significantly more time to proceed to cytokinesis, a  $\Delta gdhZ$  cell population contains many tiny cells smaller than the smallest wild-type G1 swarmer cells, a phenotype usually attributed to polar cell division events (Lutkenhaus, 2007). Surprisingly, it is unlikely to be the case for  $\Delta gdhZ$  cells as the Z-ring still assembles at midcell in the vast majority of cells (Fig 3A). Instead, it probably arises from a miscoordination between metabolism/growth and cell division. Indeed, the premature Z-ring assembly in G1 swarmer cells coupled to a slow growth rate could lead to smaller pre-divisional cells, which could *in fine* generate smaller progeny cells.

The kinetic parameters determined for GdhZ (high  $S_{0.5}$  for glutamate and low  $K_m$  for  $NAD^+$ ) suggest that the catabolic activity of GdhZ would be mainly controlled *in vivo* by glutamate availability rather than by  $NAD^+$  levels. In oligotrophic environments, amino acids could serve as a major carbon source for bacteria such as *C. crescentus*. High GDH activity could therefore be sensed as a signal of plenty for the cell division apparatus, allowing the release of daughter cells with sufficient nutrient/energy supplies. Such a mechanism would favor the survival of swarmer progeny cells in poor nutrient environments. The conservation of GdhZ among  $\alpha$ -proteobacteria also suggests that amino acids catabolism could be another common feature for these bacteria. In support of this idea, an in-frame deletion of *gdhZ* homolog in *Brucella abortus* ( $\Delta gdhZ_{Ba}$ ), an intracellular pathogen of cattle, led also to growth and cell division defects (data not shown). Moreover,  $\Delta gdhZ_{Ba}$  cells failed to sustain efficient intracellular replication in murine macrophages (F. Beaufay and R. Hallez, unpublished results), strongly suggesting that amino acids could be a major carbon source encountered by *Brucella* during infection, as it is the case for other intracellular pathogens (Zhang & Rubin, 2013). Altogether these data suggest that cell division control mediated by GdhZ could be conserved among  $\alpha$ -proteobacteria. The suppression of  $\Delta gdhZ$  defects by the addition of a GdhZ-independent carbon source (e.g. glucose) raises the possibility that (an)other enzyme(s) regulate(s) cell division according to the main carbon source encountered in the environment. It is worth to note that a connection between glycolysis and cell division has been recently highlighted in *B. subtilis* (Monahan & Hajduk, 2014). The authors proposed that pyruvate levels control Z-ring assembly thanks to the pyruvate dehydrogenase (PDH) activity (Monahan & Hajduk, 2014). As the final product of hexose (e.g. glucose) catabolism, it would be interesting to check whether pyruvate and/or PDH controls cell division in *C. crescentus* grown in the presence of glucose or other complex hexoses.

As a metabolic enzyme, GDHs are subjected to various post-translational regulations (Minambres *et al*, 2000; Commichau *et al*, 2007; Oliveira & Sauer, 2012). Our *in vitro* analysis also revealed that GDH activity of GdhZ is inhibited by TCA intermediates (e.g. citrate) and stimulated by some amino acids such as arginine (data not shown). We also observed that GdhZ auto-assembles into ordered structures (F. Beaufay and R. Hallez, unpublished results), even we do not know whether this self-assembly has any effect on GDH activity or cell division control. Self-assembly of glutamate dehydrogenase has been described for a long time in various organisms (Josephs & Borisy, 1972; O'Connell *et al*, 2012). It is worth noting that UgtP's oligomerization state was shown to play an important role in the control of cell division in *B. subtilis* (Chien *et al*, 2012).

A single protein harboring multiple functions is referred to as a "moonlighting protein" (reviewed in Huberts & van der Klei, 2010).

Moonlighting proteins are commonly found among metabolic enzymes; for example, 7 out of the 10 proteins in the glycolytic pathway and 7 out of the 8 proteins in the TCA cycle display a moonlighting function. Because of their interaction with cell metabolites and the subsequent conformational change induced upon substrate binding, metabolic enzymes constitute good candidates for signal transduction (Huberts & van der Klei, 2010).

How cells coordinate growth with cell cycle according to nutrient availability and energy supplies remains an exciting open question. Although we have now uncovered a new bifunctional enzyme that couples cell division with amino acids catabolism, further work is needed to highlight other links between metabolism and cell cycle.

## Materials and Methods

### Bacterial strains and growth conditions

*Escherichia coli* Top10 was used for cloning purpose and grown aerobically in Luria–Bertani (LB) broth (Sigma) (Casadaban & Cohen, 1980). Electrocompetent cells were used for transformation of *E. coli*. All *Caulobacter crescentus* strains used in this study are derived from the synchronizable wild-type strain NA1000 and were grown in peptone–yeast extract (PYE,) or synthetic M2 glucose (M2G) or xylose (M2X) media at 28–30°C. Growth was monitored by following the OD (600 nm) during 24 h in an automated plate reader (Bioscreen C; Lab Systems) with continuous shaking at 30°C. When indicated, media were supplemented with glucose (G), xylose (X), vanillate (Van), and alanine (A) at a final concentration of 0.2%. Genes expressed from the inducible *vanA* promoter ( $P_{vanA}$ ) were induced with 0.5 mM vanillate; genes expressed from the inducible *xylX* promoter ( $P_{xylX}$ ) were induced with  $\leq 0.05\%$  xylose in a  $\Delta xylX$  background or with 0.1% xylose in  $xylX^+$  background. For FtsZ depletion experiments, cells were grown in the presence of 0.05% xylose for induction, then washed and resuspended in PYE liquid media without xylose. Generalized transduction was performed with phage  $\Phi$ Cr30 according to the procedure described in Ely (1991).

For *E. coli*, antibiotics were used at the following concentrations ( $\mu$ g/ml; in liquid/solid medium): ampicillin (50/100), kanamycin (30/50), oxytetracycline (12.5/12.5), spectinomycin (100/100), streptomycin (50/100), and hygromycin (100/100). For *C. crescentus*, media were supplemented with kanamycin (5/20), oxytetracycline (1/2.5), spectinomycin (25/50), or streptomycin (5/5), where appropriate.

*Escherichia coli* S17-1 and *E. coli* MT607 helper strains were used for transferring plasmids to *C. crescentus* by respectively bi- and tri-parental mating. In-frame deletions were created by using the pNPTS138-derivative plasmids, by following the procedure described in Thanbichler and Shapiro (2006).

Strains and plasmids used in this study are listed in Supplementary Tables S2 and S3, together with construction details provided in the Supplementary Materials and Methods.

### Y2H screen

Y2H screen was performed using a N-terminal fragment of *C. crescentus* *ftsZ* (*ftsZ*<sub>1-324</sub>) fused to Gal4<sup>BD</sup> as bait, and a library of

random genomic DNA (gDNA) fragments of *C. crescentus* fused to Gal4<sup>AD</sup> as prey (Davis *et al*, 2013). The library was transformed into *Saccharomyces cerevisiae* strain Y187 (Clontech) and selected onto synthetic medium without leucine (SD-L). The pGBKT7-ftsZ<sub>1-324</sub> (pHR284) plasmid was transformed into *S. cerevisiae* strain Y2H Gold (Clontech) and selected onto synthetic medium without tryptophan (SD-W). Y2H screen was performed essentially as proposed by the manufacturer (Clontech). Both yeast strains were grown separately either in SD-L or in SD-W, washed, and allowed to grow together in complex rich medium supplemented with adenine for 24 h at 30°C with slow shaking. More than  $1 \times 10^7$  diploids were screened either on SD-LWH supplemented with 5 mM 3-Amino-1,2,4-triazole (3-AT) or on SD-LWA. Isolated prey plasmids were transformed into *E. coli* strain Top10 and the inserts identified by DNA sequencing.

### Immunoprecipitation

*Caulobacter crescentus* strains were grown in PYE liquid media (OD<sub>660</sub> ~0.7), harvested by centrifugation for 15 min at  $6,000 \times g$ , 4°C and resuspended in 5 ml ice-cold phosphate buffer saline (PBS) containing 0.05% Triton X-100, complete EDTA-free anti-proteases, 20 mg/ml lysozyme, 10 U/ml DNase I. Cells were first lysed by sonication, and then, zirconium beads were added and cells were disrupted by FastPrep cycles ( $5 \times 20$  s) and harvested by centrifugation for 30 min at  $14,000 \times g$ , 4°C. Cell pellets were discarded, and 1 mg of protein lysates was mixed to 50 µl of anti-FLAG M2 magnetic beads (Sigma) resuspended in PBS 20 mg/ml BSA and incubated at 4°C for 1 h. Beads were pelleted by using magnets and washed six times in PBS containing 0.05% Triton X-100. Beads were then resuspended in 100 µl SDS-loading containing 0.5 mg/ml of 3×Flag peptides (Sigma). Lysates and eluates were analyzed by Western blot. For Co-IP analysis with KidO, 0.05% xylose was added to the culture 1 h before harvesting cells, to allow *kidO-mcherry* expression.

### Immunoblot analysis

Proteins crude extracts were prepared by harvesting cells from exponential growth phase (OD<sub>660</sub> 0.1–0.4). Cells were resuspended in SDS-PAGE loading buffer and lysed by incubation at 90°C for 10 min. Proteins were then subjected to electrophoresis in a 4–15% SDS-polyacrylamide gel, transferred onto a nitrocellulose membrane, and immunoblotted for  $\geq 1$  h with primary antibodies:  $\alpha$ -FtsZ (1:20,000),  $\alpha$ -FLAG (1:5,000) (Stratagene),  $\alpha$ -CtrA (1:5,000),  $\alpha$ -MreB (1:5,000),  $\alpha$ -KidO (1:2,000) (Radhakrishnan *et al*, 2010),  $\alpha$ -GdhZ (1:10,000), and  $\alpha$ -DsRed (Clontech) (1:1,000). Membranes were then immunoblotted for  $\leq 1$  h with secondary antibodies: 1:10,000 anti-mouse (for  $\alpha$ -FLAG) or 1:7,500 anti-rabbit (for all the others) linked to peroxidase (GE Healthcare), and visualized thanks to Western Lightning Plus-ECL chemiluminescence reagent (Perkin-Elmer) and ImageQuant LAS400 (GE Healthcare).

### Synchronization of cells

For synchrony, cells were grown in 200 ml of PYE to OD<sub>660</sub> 0.6, harvested by centrifugation for 15 min at  $6,000 \times g$ , 4°C, resuspended in 60 ml of ice-cold phosphate (PO<sub>4</sub><sup>3-</sup>) buffer, and combined

with 30 ml of Ludox LS Colloidal Silica (30%) (Sigma-Aldrich) (Jenal & Shapiro, 1996). Cells resuspended in Ludox were centrifuged for 40 min at  $9,000 \times g$ , 4°C. Swarmer cells, corresponding to the bottom band, were isolated, washed twice in ice-cold PO<sub>4</sub><sup>3-</sup> buffer, and finally resuspended in prewarmed PYE media for growth at 30°C. Samples were collected every 15 min for Western blot, microscopy, and FACS analyses.

### Light and fluorescent microscopy

All strains were imaged during exponential growth phase after immobilization on 1% agarose pads (Ely, 1991). For time-lapse experiments, cells were grown in PYE, transferred onto freshly prepared PYE 1.5% agarose pads, covered, and sealed with 1:1:1 mixture of paraffin, lanolin, and vaseline. Microscopy was performed using Axioskop microscope (Zeiss), Orca Flash 4.0 camera (Hamamatsu), and Zen 2012 software (Zeiss). Images were processed with ImageJ.

### Microbetracker and matlab analysis

Cell identification and analysis were obtained using the Matlab-based open-source software MicrobeTracker. Further quantitative analyses from cell meshes were performed with Matlab software (The MathWorks Inc., Natick, MA). Demographic representations were created using scripts derived from Hocking *et al* (2012). Briefly, each cell was sorted by length and segmented, and fluorescence in each segment was integrated, normalized to the brightest segment, and plotted as a heat map from 0 (no fluorescence) to 1 (maximum fluorescence). Polar and midcell signals were considered when a maximal fluorescence ( $\geq 1.5$ -fold of the mean fluorescence) was localized up to 0.1 from each pole (0–0.1; 0.9–1) or from 0.4 to 0.6, respectively.

### Proteins purification

FtsZ purification was performed as described in Thanbichler and Shapiro (2006).

GdhZ purification was performed essentially as described in Minambres *et al* (2000) with the exception of GdhZ overproduction. *Escherichia coli* BL21 (DE3) was transformed with plasmid pHR354 (pET-21b-*gdhZ*) or pHR573 (pET-21b-*gdhZ*<sub>K837A</sub>) and grown to an OD<sub>600</sub> of ~0.6 in LB medium (2 L) at 37°C. Isopropyl- $\beta$ -D-thiogalactoside (IPTG) was added to a final concentration of 1 mM and incubated for 4 h. Cells were harvested by centrifugation for 30 min at  $5,000 \times g$ , 4°C. Following purification, samples were dialyzed in 50 mM HEPES, pH 7.2, 50 mM KCl, 10 mM MgCl<sub>2</sub>, 10% glycerol, 5 mM  $\beta$ -mercaptoethanol, and aliquoted, snap-frozen in liquid N<sub>2</sub>, and stored at –80°C. Purified GdhZ was also used to immunize a rabbit in order to produce  $\alpha$ -GdhZ polyclonal antibodies.

To purify KidO, *E. coli* BL21 (DE3) was transformed with pHR624 (pET-21b-*kidO*) and grown to an OD<sub>600</sub> of 0.6 in LB medium (2 L) at 37°C. IPTG was added to a final concentration of 1 mM and incubated for 4 h. Cells were harvested by centrifugation for 30 min at  $5,000 \times g$ , 4°C. Cells were resuspended in 20 ml of buffer A (50 mM Tris, pH 8.5, 1 mM ethylenediaminetetraacetic acid (EDTA), 10% glycerol, 100 µg/ml phenylmethylsulfonyl fluoride (PMSF) containing 10 U/ml DNase I and complete EDTA-free anti-proteases (Roche)). Resuspended cells were then disrupted by

sonication and cell debris pelleted by centrifugation for 30 min at  $37,000 \times g$ , 4°C. The supernatant was then passed through HiTrap DEAE Fast Flow columns (Sigma,  $2 \times 5$  ml) equilibrated with buffer A. Columns were washed with 100 ml of buffer A, and elution was carried out with buffer A2 (buffer A + 80 mM KCl). Aliquots of 3 ml were collected at a flow rate of 3 ml/min. Fractions containing the KidO were detected by SDS-PAGE and Coomassie blue staining. These fractions were pooled, dialyzed for 24 h in 50 mM HEPES, pH 7.5, 50 mM KCl, 10 mM MgCl<sub>2</sub>, 10% glycerol, 5 mM β-mercaptoethanol, and aliquoted, snap-frozen in liquid N<sub>2</sub>, and stored at -80°C.

In order to immunize rabbits for production of specific polyclonal antibodies, His6-MreB<sub>142-347</sub>, FtsZ-His6, and His6-CtrA were purified according to published works (Quon *et al*, 1996; Quardokus *et al*, 2001; Figge *et al*, 2004).

### GTPase assay

The GTPase activity of FtsZ was assayed with the GTPase Assay Kit (Innova Biosciences, high fidelity) following the manufacturer's protocol. GTPase assays were performed with 0.5 μM FtsZ or FtsZ<sub>E79K</sub> in polymerization buffer (50 mM HEPES pH 7.2, 50 mM KCl, 0.1 mM EDTA, 1 mM β-mercaptoethanol, 10 mM MgCl<sub>2</sub>). Reactions were started by the addition of 1 mM GTP before adding KidO and/or GdhZ or GdhZ<sub>K837A</sub>. When present, NAD<sup>+</sup> and glutamate were used at a final concentration of 5 mM and 100 mM, respectively. Hydrolysis rates were calculated from the slope of the P<sub>i</sub> values plotted according to time. P<sub>i</sub> values were normalized according to corresponding blank conditions containing all reagents except GTP.

### Electron microscopy

As for GTPase assays, reactions were performed with 0.5 μM FtsZ in polymerization buffer and initiated by addition of 1 mM GTP. Polymerization mixtures were incubated for 5 min at RT. Samples were then applied to glow-discharged carbon-coated grids, stained with 2% uranyl acetate for 1 min, washed with a drop of distilled water, blotted, and air-dried. Images were taken at 80 kV on a TECNAI 10 transmission electron microscope with a Gatan 967 slow-scan, cooled CCD camera.

### β-Galactosidase assay

Cells resuspended in 800 μl of Z buffer (60 mM Na<sub>2</sub>HPO<sub>4</sub>, 40 mM NaH<sub>2</sub>PO<sub>4</sub>, 10 mM KCl, 1 mM MgSO<sub>4</sub>) were lysed with chloroform. After the addition of 200 μl ONPG (4 mg/ml), reactions were incubated at 30°C until color turned yellowish. Reactions were then stopped by the addition of 500 μl of 1 M Na<sub>2</sub>CO<sub>3</sub>, and absorbance at 420 nm was measured. Miller units are defined as  $(OD_{420} \times 1,000) / (OD_{660} \times t \times v)$ , where "OD<sub>660</sub>" is the absorbance at 660 nm of the cultures before the β-galactosidase assays, "t" is the time of the reaction (min), and "v" is the volume of cultures used in the assays (ml). All the experiments were performed with three biological replicates and were normalized according to the wild-type strain harboring the P<sub>gdhZ</sub>-lacZ fusion cultivated at 30°C.

**Supplementary information** for this article is available online: <http://emboj.embopress.org>

### Acknowledgements

We are grateful to Yves Brun, Patrick Viollier, Christine Jacobs-Wagner, Martin Thanbichler, and Urs Jenal for providing antibodies, strains, and plasmids. We further thank Urs Jenal for sharing the yeast two-hybrid library. We thank Jean-Yves Matroule and the members of the BCcD team for critical reading of the manuscript and helpful discussions; Joanne Lau and Peter Chien for helpful discussions and suggestions about ClpXP-dependent proteolysis; David Delgleize and Corry Charlier at the Electron Microscopy Service of the University of Namur for assistance with the transmission electron microscope; and Guy Houbeau at the Animal Care Facility of the University of Namur for immunizing rabbits with purified proteins. F.B. and J.C. hold a FRIA (Fund for Research Training in Industry and Agriculture) fellowship from the National Fund for Scientific Research (F.R.S.-FNRS) and R.H. was holding a Postdoctoral Researcher from the F.R.S.-FNRS. This work was supported by a Research Project (PDR T.0053.13) to X.D.B and a Research Credit (CDR 1.5067.12) to R.H. from the F.R.S.-FNRS.

### Author contributions

FB and RH conceived and designed the experiments. FB performed all the experiments except otherwise stated. JC did the Y2H screen and constructed the ΔgdhZ mutant. AM purified all the native proteins. GL performed the quantitative analysis on Matlab software. FB, XDB, and RH analyzed the data and contributed reagents/materials/analysis tools. FB and RH wrote the manuscript.

### Conflict of interest

The authors declare that they have no conflict of interest.

### References

- Aakre CD, Phung TN, Huang D, Laub MT (2013) A bacterial toxin inhibits DNA replication elongation through a direct interaction with the β sliding clamp. *Mol Cell* 52: 617–628
- Aaron M, Charbon G, Lam H, Schwarz H, Vollmer W, Jacobs-Wagner C (2007) The tubulin homologue FtsZ contributes to cell elongation by guiding cell wall precursor synthesis in *Caulobacter crescentus*. *Mol Microbiol* 64: 938–952
- Abel S, Chien P, Wassmann P, Schirmer T, Kaefer V, Laub MT, Baker TA, Jenal U (2011) Regulatory cohesion of cell cycle and cell differentiation through interlinked phosphorylation and second messenger networks. *Mol Cell* 43: 550–560
- Arentson BW, Sanyal N, Becker DF (2012) Substrate channeling in proline metabolism. *Front Biosci* 17: 375–388
- Bernhardt TG, de Boer PAJ (2005) SlmA, a nucleoid-associated, FtsZ binding protein required for blocking septal ring assembly over chromosomes in *E. coli*. *Mol Cell* 18: 555–564
- Campos M, Surovtsev IV, Kato S, Paintdakhi A, Beltran B, Ebmeier SE, Jacobs-Wagner C (2014) A constant size extension drives bacterial cell size homeostasis. *Cell* 159: 1433–1446
- Casadaban MJ, Cohen SN (1980) Analysis of gene control signals by DNA fusion and cloning in *Escherichia coli*. *J Mol Biol* 138: 179–207
- Chien A-C, Zareh SKG, Wang YM, Levin PA (2012) Changes in the oligomerization potential of the division inhibitor UgtP co-ordinate *Bacillus subtilis* cell size with nutrient availability. *Mol Microbiol* 86: 594–610
- Commichau FM, Herzberg C, Tripal P, Valerius O, Stulke J (2007) A regulatory protein-protein interaction governs glutamate biosynthesis in *Bacillus*

- subtilis*: the glutamate dehydrogenase RocG moonlights in controlling the transcription factor GltC. *Mol Microbiol* 65: 642–654
- Dajkovic A, Pichoff S, Lutkenhaus J, Wirtz D (2010) Cross-linking FtsZ polymers into coherent Z rings. *Mol Microbiol* 78: 651–668
- Davis NJ, Cohen Y, Sanselicio S, Fumeaux C, Ozaki S, Luciano J, Guerrero-Ferreira RC, Wright ER, Jenal U, Viollier PH (2013) De- and repolarization mechanism of flagellar morphogenesis during a bacterial cell cycle. *Genes Dev* 27: 2049–2062
- Degnen ST, Newton A (1972) Chromosome replication during development in *Caulobacter crescentus*. *J Mol Biol* 64: 671–680
- Domian IJ, Quon KC, Shapiro L (1997) Cell type-specific phosphorylation and proteolysis of a transcriptional regulator controls the G1-to-S transition in a bacterial cell cycle. *Cell* 90: 415–424
- Duerig A, Abel S, Folcher M, Nicollier M, Schwede T, Amiot N, Giese B, Jenal U (2009) Second messenger-mediated spatiotemporal control of protein degradation regulates bacterial cell cycle progression. *Genes Dev* 23: 93–104
- Dunn MF (2012) Allosteric regulation of substrate channeling and catalysis in the tryptophan synthase holoenzyme complex. *Arch Biochem Biophys* 519: 154–166
- Ely B (1991) Genetics of *Caulobacter crescentus*. *Methods Enzymol* 204: 372–384
- Erickson HP, Stoffler D (1996) Protofilaments and rings, two conformations of the tubulin family conserved from bacterial FtsZ to alpha/beta and gamma tubulin. *J Cell Biol* 135: 5–8
- Erickson HP, Anderson DE, Osawa M (2010) FtsZ in bacterial cytokinesis: cytoskeleton and force generator all in one. *Microbiol Mol Biol Rev* 74: 504–528
- Figge RM, Divakaruni AV, Guber JW (2004) MreB, the cell shape-determining bacterial actin homologue, co-ordinates cell wall morphogenesis in *Caulobacter crescentus*. *Mol Microbiol* 51: 1321–1332
- Fumeaux C, Radhakrishnan SK, Ardisson S, Theraulaz L, Frandi A, Martins D, Nesper J, Abel S, Jenal U, Viollier PH (2014) Cell cycle transition from S-phase to G1 in *Caulobacter* is mediated by ancestral virulence regulators. *Nat Commun* 5: 4081
- Goehring NW, Beckwith J (2005) Diverse paths to midcell: assembly of the bacterial cell division machinery. *Curr Biol* 15: R514–R526
- Goley ED, Dye NA, Werner JN, Gitai Z, Shapiro L (2010) Imaging-based identification of a critical regulator of FtsZ protofilament curvature in *Caulobacter*. *Mol Cell* 39: 975–987
- Goley ED, Yeh Y-C, Hong S-H, Fero MJ, Abeliuk E, McAdams HH, Shapiro L (2011) Assembly of the *Caulobacter* cell division machine. *Mol Microbiol* 80: 1680–1698
- Gonzalez JM, Jimenez M, Velez M, Mingorance J, Andreu JM, Vicente M, Rivas G (2003) Essential cell division protein FtsZ assembles into one monomeric thick ribbons under conditions resembling the crowded intracellular environment. *J Biol Chem* 278: 37664–37671
- Hill NS, Buske PJ, Shi Y, Levin PA (2013) A Moonlighting enzyme links *Escherichia coli* cell size with central metabolism. *PLoS Genet* 9: e1003663
- Hocking J, Priyadarshini R, Takacs CN, Costa T, Dye NA, Shapiro L, Vollmer W, Jacobs-Wagner C (2012) Osmolality-dependent relocation of penicillin-binding protein PBP2 to the division site in *Caulobacter crescentus*. *J Bacteriol* 194: 3116–3127
- Holden SJ, Pengo T, Meibom KL, Fernandez Fernandez C, Collier J, Manley S (2014) High throughput 3D super-resolution microscopy reveals *Caulobacter crescentus* in vivo Z-ring organization. *Proc Natl Acad Sci USA* 111: 4566–4571
- Huberts DHEW, van der Klei IJ (2010) Moonlighting proteins: an intriguing mode of multitasking. *Biochim Biophys Acta* 1803: 520–525
- Hughes HV, Huitema E, Pritchard S, Keiler KC, Brun YV, Viollier PH (2010) Protein localization and dynamics within a bacterial organelle. *Proc Natl Acad Sci USA* 107: 5599–5604
- Hughes HV, Lisher JP, Hardy GG, Kysela DT, Arnold RJ, Giedroc DP, Brun YV (2013) Co-ordinate synthesis and protein localization in a bacterial organelle by the action of a penicillin-binding-protein. *Mol Microbiol* 90: 1162–1177
- Huitema E, Pritchard S, Matteson D, Radhakrishnan SK, Viollier PH (2006) Bacterial birth scar proteins mark future flagellum assembly site. *Cell* 124: 1025–1037
- Iniesta AA, McGrath PT, Reisenauer A, McAdams HH, Shapiro L (2006) A phospho-signaling pathway controls the localization and activity of a protease complex critical for bacterial cell cycle progression. *Proc Natl Acad Sci USA* 103: 10935–10940
- Jenal U, Shapiro L (1996) Cell cycle-controlled proteolysis of a flagellar motor protein that is asymmetrically distributed in the *Caulobacter* predivisional cell. *EMBO J* 15: 2393–2406
- Josephs R, Borisy G (1972) Self-assembly of glutamic dehydrogenase into ordered superstructures: multichain tubes formed by association of single molecules. *J Mol Biol* 65: 127–155
- Karsenti E, Vernos I (2001) The mitotic spindle: a self-made machine. *Science* 294: 543–547
- Kelly AJ, Sackett MJ, Din N, Quardokus E, Brun YV (1998) Cell cycle-dependent transcriptional and proteolytic regulation of FtsZ in *Caulobacter*. *Genes Dev* 12: 880–893
- Kirkpatrick CL, Viollier PH (2011) New(s) to the (Z)-ring. *Curr Opin Microbiol* 14: 691–697
- Lam H, Schofield WB, Jacobs-Wagner C (2006) A landmark protein essential for establishing and perpetuating the polarity of a bacterial cell. *Cell* 124: 1011–1023
- Laporte D, Zhao R, Wu J-Q (2010) Mechanisms of contractile-ring assembly in fission yeast and beyond. *Semin Cell Dev Biol* 21: 892–898
- Laub MT, McAdams HH, Feldblyum T, Fraser CM, Shapiro L (2000) Global analysis of the genetic network controlling a bacterial cell cycle. *Science* 290: 2144–2148
- Li H-Y, Zheng Y (2004) Phosphorylation of RCC1 in mitosis is essential for producing a high RanGTP concentration on chromosomes and for spindle assembly in mammalian cells. *Genes Dev* 18: 512–527
- Li Z, Trimble MJ, Brun YV, Jensen GJ (2007) The structure of FtsZ filaments *in vivo* suggests a force-generating role in cell division. *EMBO J* 26: 4694–4708
- Lutkenhaus J (2007) Assembly dynamics of the bacterial MinCDE system and spatial regulation of the Z ring. *Annu Rev Biochem* 76: 539–562
- Margolin W (2000) Themes and variations in prokaryotic cell division. *FEMS Microbiol Rev* 24: 531–548
- Margolin W (2009) Sculpting the bacterial cell. *Curr Biol* 19: R812–R822
- Martin ME, Trimble MJ, Brun YV (2004) Cell cycle-dependent abundance, stability and localization of FtsA and FtsQ in *Caulobacter crescentus*. *Mol Microbiol* 54: 60–74
- McGrath PT, Iniesta AA, Ryan KR, Shapiro L, McAdams HH (2006) A dynamically localized protease complex and a polar specificity factor control a cell cycle master regulator. *Cell* 124: 535–547
- Minambres B, Olivera ER, Jensen RA, Luengo JM (2000) A new class of glutamate dehydrogenases (GDH). Biochemical and genetic characterization of the first member, the AMP-requiring NAD-specific GDH of *Streptomyces clavuligerus*. *J Biol Chem* 275: 39529–39542
- Monahan LG, Robinson A, Harry EJ (2009) Lateral FtsZ association and the assembly of the cytokinetic Z ring in bacteria. *Mol Microbiol* 74: 1004–1017

- Monahan LG, Hajduk IV (2014) Coordinating bacterial cell division with nutrient availability: a role for glycolysis. *mBio* 5: e00935–14
- Mukherjee A, Lutkenhaus J (1994) Guanine nucleotide-dependent assembly of FtsZ into filaments. *J Bacteriol* 176: 2754–2758
- O'Connell JD, Zhao A, Ellington AD, Marcotte EM (2012) Dynamic reorganization of metabolic enzymes into intracellular bodies. *Annu Rev Cell Dev Biol* 28: 89–111
- Oliveira AP, Sauer U (2012) The importance of post-translational modifications in regulating *Saccharomyces cerevisiae* metabolism. *FEMS Yeast Res* 12: 104–117
- Osawa M, Erickson HP (2011) Inside-out Z rings—constriction with and without GTP hydrolysis. *Mol Microbiol* 81: 571–579
- Osley MA, Newton A (1980) Temporal control of the cell cycle in *Caulobacter crescentus*: roles of DNA chain elongation and completion. *J Mol Biol* 138: 109–128
- Osteryoung KW (2001) Organelle fission in eukaryotes. *Curr Opin Microbiol* 4: 639–646
- Quardokus EM, Din N, Brun YV (2001) Cell cycle and positional constraints on FtsZ localization and the initiation of cell division in *Caulobacter crescentus*. *Mol Microbiol* 39: 949–959
- Quon KC, Marczyński GT, Shapiro L (1996) Cell cycle control by an essential bacterial two-component signal transduction protein. *Cell* 84: 83–93
- Radhakrishnan SK, Pritchard S, Viollier PH (2010) Coupling prokaryotic cell fate and division control with a bifunctional and oscillating oxidoreductase homolog. *Dev Cell* 18: 90–101
- Sargent MG (1975) Control of membrane protein synthesis in *Bacillus subtilis*. *Biochim Biophys Acta* 406: 564–574
- Schendel FJ, Cheng YS, Otvos JD, Wehrli S, Stubbe J (1988) Characterization and chemical properties of phosphoribosylamine, an unstable intermediate in the *de novo* purine biosynthetic pathway. *Biochemistry* 27: 2614–2623
- Sliusarenko O, Heinritz J, Emonet T, Jacobs-Wagner C (2011) High-throughput, subpixel precision analysis of bacterial morphogenesis and intracellular spatio-temporal dynamics. *Mol Microbiol* 80: 612–627
- Stricker J, Maddox P, Salmon ED, Erickson HP (2002) Rapid assembly dynamics of the *Escherichia coli* FtsZ-ring demonstrated by fluorescence recovery after photobleaching. *Proc Natl Acad Sci USA* 99: 3171–3175
- Szwedziak P, Wang Q, Bharat TA, Tsim M, Lowe J (2014) Architecture of the ring formed by the tubulin homologue FtsZ in bacterial cell division. *eLife* 3: e04601
- Thanbichler M, Shapiro L (2006) MipZ, a spatial regulator coordinating chromosome segregation with cell division in *Caulobacter*. *Cell* 126: 147–162
- Weart RB, Lee AH, Chien A-C, Haeusser DP, Hill NS, Levin PA (2007) A metabolic sensor governing cell size in bacteria. *Cell* 130: 335–347
- Wu LJ, Errington J (2004) Coordination of cell division and chromosome segregation by a nucleoid occlusion protein in *Bacillus subtilis*. *Cell* 117: 915–925
- Yokoyama H, Gruss OJ (2013) New mitotic regulators released from chromatin. *Front Oncol* 3: 308
- Zhang YJ, Rubin EJ (2013) Feast or famine: the host-pathogen battle over amino acids. *Cell Microbiol* 15: 1079–1087